HHS Public Access

Author manuscript

Cell Host Microbe. Author manuscript; available in PMC 2017 March 09.

Published in final edited form as:

Cell Host Microbe. 2016 March 09; 19(3): 388–399. doi:10.1016/j.chom.2016.02.009.

Bacterial Peptidoglycan Traverses the Placenta to Induce Fetal Neuroproliferation and Aberrant Postnatal Behavior

Jessica Humann[1,3,*], **Beth Mann**[1,*], **Geli Gao**[1], **Philip Moresco**[1], **Joseph Ramahi**[1], **Lip Nam Loh**[1], **Arden Farr**[1], **Yunming Hu**[1,4], **Kelly Durick-Eder**[1,5], **Sophie A. Fillon**[1,6], **Richard J. Smeyne**[2], and **Elaine I. Tuomanen**[1,**]

[1]Department of Infectious Diseases, St. Jude Children's Research Hospital, Memphis, TN

[2]Department of Neurobiology, St. Jude Children's Research Hospital, Memphis, TN

Summary

Maternal infection during pregnancy is associated with adverse outcomes for the fetus, including postnatal cognitive disorders. However, the underlying mechanisms are obscure. We find that bacterial cell wall peptidoglycan (CW), a universal PAMP for TLR2, traverses across the murine placenta into the developing fetal brain. In contrast to adults, CW-exposed fetal brains did not show any signs of inflammation or neuronal death. Instead, the neuronal transcription factor FoxG1 was induced and neuroproliferation leading to a 50% greater density of neurons in the cortical plate was observed. Bacterial infection of pregnant dams followed by antibiotic treatment, which releases CW, yielded the same result. Neuroproliferation required TLR2 and was recapitulated in vitro with fetal neuronal precursor cells and TLR2/6, but not TLR2/1 ligands. The fetal neuroproliferative response correlated with abnormal cognitive behavior in CW-exposed pups following birth. Thus, the bacterial CW-TLR2 signaling axis affects fetal neurodevelopment and may underlie postnatal cognitive disorders.

Introduction

Infection and inflammation during pregnancy have been associated with adverse outcomes such as preterm birth, abortion and postnatal cognitive disorders (Lowe et al. 2008, Sorenson

**Corresponding author: Elaine Tuomanen, M.D., St. Jude Children's Research Hospital, 262 Danny Thomas Place, Mail Stop 320, Memphis, TN 38105, Tel.: (901) 495-3114, Fax: (901) 495-3099, elaine.tuomanen@stjude.org.

[3]Current addresses:
Department of Biology, Florida Agricultural and Mechanical University, Tallahassee, FL, 32307; jessica.humann@famu.edu

[4]Electron Microscopy Facility, Trinity College, Hartford, CT, 06106; yunming_hu@hotmail.com

[5]Department of Biology, College of St. Scholastica, Duluth, MN, 55811; kdurickeder@css.edu

[6]Department of Pediatrics, University of Colorado Denver, School of Medicine, Aurora, CO 80045; sophie.fillon@ucdenver.edu

*Co-first authors

The authors have no conflicts of interest to disclose.

Author contributions

Conceptualization, E.I.T.; Methodology, J.H., B.M., Y.H., J. R. and R.J.S.; Investigation, J.H., B.M., G.G., P.M., L.N.L, A.F., Y.H., J. R. K.D-E., and S.A.F; Writing – Original Draft, J.H., B.M., and E.I.T.; Writing – Review & Editing, J.H., B.M., L.N.L, and R.J.S.; Funding Acquisition, E.I.T.; Resources, R.J.S.; Supervision, R.J.S. and E.I.T.

et al. 2008, Canetta et al. 2014). Yet, how microbial products circulating in the maternal bloodstream affect fetal development is poorly understood. The disruptive effects of inflammation would be substantial as fetal organs undergo complex waves of proliferation and apoptosis during gestation (Couzin-Frankel, 2013; Roth and D'Sa, 2001). Microbial components display pathogen associated molecular patterns (PAMPs) that are recognized by the innate immune system and serve to trigger inflammation. In Gram positive bacteria, cell wall (CW) is a complex exopolymer that harbors several PAMPs that potently activate inflammation when released into the bloodstream during bacterial infection or when explosively discharged during bacterial lysis by common antibiotics (Tuomanen et al 1985a,b). CW binds to innate immune Toll-like receptors (TLRs), particularly TLR2, and initiates signaling leading to inflammation by a well recognized cascade involving MyD88, NFkB and cytokine secretion (Aliprantis et al., 1999; Yoshimura et al., 1999). This signaling process underlies the pathogenesis of bacterial meningitis where CW/TLR2 ligation provokes a broad spectrum of acute signs and symptoms of brain inflammation (Orihuela et al., 2006; Tuomanen et al., 1985a,b). In children and adults with pneumococcal meningitis, neuronal death predominates (Braun et al., 1999; Braun et al., 2001; Mitchell et al., 2004) and neuroproliferation is insufficient to repair brain injury, leaving survivors with devastating permanent sequelae, such as paralysis, seizures, and memory loss (Gerber et al., 2003; Hoffmann et al., 2007). The degree of damage depends on the pathogen, with pneumococci considered the most severe (Schmidt et al., 2006).

TLR2 is abundant in the embryo (Okun et al, 2010) but little is known of the outcome of activation of this cascade in the fetus. It is unknown if TLR2 ligands, such as CW, cross the placenta. Bacterial CW could be an important participant in microbial-host signaling at the maternal-fetal interface since CW circulates in the maternal bloodstream not only during infection but also from the microbiome in healthy mothers (Clarke et al., 2010). There is an emerging awareness of complex communication ongoing between the microbiome and the brain (Collins et al., 2012; Tracey, 2009) that modulates a variety of complex human behaviors and patterning of neuronal circuitry (Collins et al., 2012; Cryan and Dinan, 2012; Hsiao et al., 2013). Early neurodevelopmental stress and autism spectrum disorders have been linked to gut microbial dysbiosis (Hsiao et al., 2013).

We sought to use concepts of the pathogenesis of bacterial meningitis and CW-induced innate signaling to develop a model to probe the impact of bacterial products on fetal brain development. Since CW components traffic from blood across the blood brain barrier and induce neuroinflammation in the adult (Fillon et al., 2006), we reasoned that such a model, when extended to pregnant mice, could be used to test the ability of bacterial CW to cross the placenta and inform the capacity of the fetal brain to respond directly to bacterial PAMPs. This information would be relevant to general questions concerning the developing brain, such as the nature of the TLR2 response in the fetal brain and the potential for microbial products to affect neurodevelopment.

Our data indicate that the placenta allows CW traffic from the maternal to the fetal circulation. In contrast to neuronal death seen in the postnatal scenario (Tuomanen et al., 1985a,b; Nau and Bruck, 2002), engagement of TLR2 by CW in the fetus results in robust

FoxG1-dependent neuroproliferation. This *in utero* response alters cerebral anatomy and appears have long-term postnatal behavioral consequences.

Results

Interaction of CW with the placenta

The peptidoglycan-teichoic acid complex of the CW of *Streptococcus pneumoniae* was chosen as a prototype component of Gram-positive bacteria that incites inflammation via the innate immune receptor TLR2 (Yoshimura et al., 1999) and whose bioactivities in the brain have been well characterized (Tuomanen et al., 1985a,b; Fillon et al., 2006; Orihuela et al., 2006). To investigate bioactivities of CW in the placenta, this macromolecule was fractionated, purified free of protein adducts, labeled with FITC, and injected intravenously into pregnant dams on embryonic day 15 (E15). FITC-CW was detected in placental tissue within 10 min of maternal administration and accumulated by 24hrs (Fig. 1A).

Bacterial components decorated with phosphorylcholine, a modification present on most oral commensals and respiratory pathogens, bind by molecular mimicry to the G-protein coupled platelet activating factor receptor (PAFr) (Cundell et al., 1995). In the case of pneumococcus, phosphorylcholine covalently modifies the CW, and the interaction between CW and PAFr supports uptake of both free CW and intact pneumococci into eukaryotic cells and across cellular barriers (Fillon et al., 2006). PAFr is expressed extensively in the fetal brain and placenta (Supplementary Fig. 1SA; Okun et al. 2010)). When examined in $PAFr^{-/-}$ mice, significantly fewer FITC-CW particles accumulated in placental tissue (Fig 1A) indicating that this mechanism of translocation across host boundaries by bacterial components operates in the placenta. This was further supported *in vitro* by robust association of CW with trophoblast cells contrasted by a rare association of EA CW, where ethanolamine was substituted for phosphorylcholine (Supplementary Fig 1SB).

Many organs undergo apoptosis upon postnatal exposure to CW (Braun et al., 1999; Orihuela et al., 2006). In contrast, examination of the placenta after CW administration to wild type mice showed only a modest increase in both $TUNEL^{+}$ and caspase-3^{+} cells (Fig. 1B, C). In $TLR2^{-/-}$ mice, CW-induction of death in the placenta was not significantly different from PBS (Fig. 1B, C; Supplementary Fig. 1SC). CW caused no immediate fetal distress, as measured by umbilical vein velocity and fetal heart rate (Fig. 1D, E). All CW and PBS treated embryos were equally viable at birth and had similar weights at the time of weaning (mean ± SD: 10.4g ± 0.4 and 9.8g ± 0.3, CW and PBS respectively; n = 12 per group; p = 0.27). Thus, CW trafficked to placental tissue via PAFr but did not induce strong cell death responses.

CW enters the developing fetal brain

In postnatal animal models, CW fragments in the bloodstream distribute across the blood brain barrier and induce signs and symptoms of meningitis (Tuomanen et al., 1985a,b) accompanied by extensive neuronal death (Braun et al., 1999; Braun et al., 2001). To determine if a similar pathology occurred in the developing brain, CW was administered intravenously to pregnant dams and localization of CW was examined in the embryonic

cortex. CW injected in a single dose at E10 or E15 was detected in the fetal brain 24hrs later (Fig. 2A). A cell wall density of ~400 pieces/mm^2 corresponds to 4 × 10^5 pieces per entire cortical plate indicating that ~2% of the inoculum into mother trafficked to the fetal brain. CW administered daily from E10-E14 was present in the cortex at E16 at similar levels to that seen in a single E15 injection (Fig. 2A). However, accumulation may be transient since a single dose of CW injected at E10 was not visible in the brain at E16 (Fig. 2A). EA CW that crosses the blood brain barrier poorly (lacks phosphorylcholine), was not detected in the fetal brain (data not shown). TLR2$^{-/-}$ fetal brains showed equivalent accumulation of CW as WT; in contrast, PAFr$^{-/-}$ fetal brains exhibited significantly less CW accumulation (Fig. 2B). In addition to the cortex, pneumococcal CW was found in multiple regions of the developing fetal brain, including the cerebellum, olfactory region, thalamus, and choroid plexus (data not shown). Thus, CW readily enters the developing fetal brain in a PAFr-dependent manner previously well-established in the postnatal brain (Cundell et al., 1995).

CW-induced neuronal fate decisions in the embryonic brain

Extensive neuronal cell death is evident in brains of humans with meningitis and in postnatal mouse models using living bacteria or intravenous CW components (Fillon et al., 2006; Nau and Bruck, 2002). In the animal models, intravenous challenge with 10^7 living pneumococci or 10^7 bacterial equivalents of cell wall induces high levels of neuronal apoptosis by 24 hours (58 ± 6 and 54 ± 7 apoptotic cells/mm^2, respectively; Fig. 2C) (Orihuela et al., 2006). However, exposure of the fetus to CW caused only low level TUNEL$^+$ cell death compared to adult brains and no significant increase in caspase-3$^+$ staining (Fig. 2C, D). No increase in cell death was seen in TLR2$^{-/-}$ and PAFr$^{-/-}$ mice (Supplementary Fig. 2S). Microglial activation as indicated by the marker Iba-1 was strong in adult brain post CW while the fetus showed a decrease in this inflammatory marker post CW (Fig. 2E).

Rather than cell death, the response of the fetal brain to CW revealed marked neuronal proliferation. In the cortex, the area and cell density of the cortical plate was measured using stereology with the Cavalieri estimator and the optical fractionator probe (Fig. 3A, B). For embryos exposed to CW at E10 and analyzed at E16, the area of the cortical plate remained stable (1.05×10^6 ± 0.16 vs 1.09×10^6 ± 0.14 μm^2 PBS) but a 50% increase in density of neurons was observed (Fig. 3B, C left panel). This increased cell density was absent in TLR2$^{-/-}$ or PAFr$^{-/-}$ mice (Fig. 3B, C left panel) or in embryos challenged at E15 and harvested at E16 with wild type CW.

To extend this observation to a more clinically relevant scenario, blood stream infection with *S. pneumoniae* was established in E9 pregnant dams followed by daily treatment until E16 by ampicillin, known to potently release cell wall and contents by lysis (Tuomanen et al., 1985a,b). Embryos thus exposed to CW debris showed a significant increase in density of cortical plate neurons compared to ampicillin alone (Fig. 3C right panel). Embryos exposed to maternal infection treated with clindamycin, a protein synthesis inhibitor that does not release cell wall, showed no increase in cortical neuronal density (Fig. 3C right panel).

New neurons originate deep in the cortical ventricular zone and migrate out to the superficial cortical plate. To document the effect of CW exposure on immature neurons (Yamaguchi et al., 2000), pregnant Nestin-GFP transgenic dams were treated with CW and the Nestin-GFP

signal in the fetal brain, was visualized via fluorescence microscopy. CW exposure strongly enhanced the GFP signal in immature neurons of the ventricular zone of the developing cortex (Fig. 3D; quantitation shown in Supplementary Fig. 3S, p=0.035). PAFr$^{-/-}$ embryos showed no proliferation consistent with the absence of CW entering the brain. Furthermore, expression of TLR2, the innate immune receptor for CW, was required for neuronal proliferation, as TLR2 -deficient embryos did not show a significant increase in Nestin-GFP signal post-CW exposure (Fig. 3D).

To further confirm that CW exposure induced neuronal proliferation in the developing brain, E15 pregnant FUCCI mice, that express genetically encoded markers for the cell cycle transition from G1 to S phase (Sakaue-Sawano et al., 2008), were challenged with CW and dual color intensity of the fetal cortex was analyzed 24hrs later (Fig. 3E). The number of geminin positive dividing cells was significantly increased in the ventricular zone of the fetal cortex post-CW exposure. Immunohistochemical tracking of phosphohistone H3, a general marker of neuronal proliferation, revealed that CW induced a highly significant tripling of proliferating cells in the ventricular zone (Fig. 3F: mean ±SD MFI 319% ± 50 over PBS baseline of 100% ± 62; p= 0.0003). Taken together, results indicate that exposure of embryos to CW from the maternal circulation induces neuroproliferation in the ventricular zone of the cortex that results in an increased cell density in the cortical plate.

In vitro assay of CW-induced neuroproliferation

To examine the mechanism of the fetal cell response to CW, neuronal precursor cells (NPCs) from fetal brain were harvested and proliferation after CW challenge *in vitro* was measured either by direct counting by microscopy, by incorporation of BrdU or by loading with CFSE label followed by FACS to quantify dilution of the CFSE signal as cells divided. Using the CSFE assay, CW clearly induced a shift from bright to dim cells compared to PBS treatment indicating active cell division (Fig. 4A), while TLR2$^{-/-}$ and PAFr$^{-/-}$ NPCs failed to proliferate (Fig. 4B). Direct visual enumeration confirmed CFSE assay proliferation (Supplementary Fig. 4SA). Incorporation of BrdU as a proliferation marker also clearly indicated wild type cells proliferated strongly, while PAFr$^{-/-}$ cells showed a low but detectable response and TLR2$^{-/-}$ cells showed no response (Supplementary Fig. 4SB). The degree of proliferation correlated directly with the CW dose but was independent of the timing of the NPC harvest between E12 and E14 (Supplementary Fig. 4SC). Living pneumococci (deficient in the toxin pneumolysin) treated with ampicillin but not clindamycin also induced proliferation (Supplementary Fig. 4SD). Staphylococcal peptidoglycan also induced proliferation (ranging between 20 to 30% of cells above PBS baseline) supporting the general relevance of cell wall/TLR2 signaling. To determine if chemically distinct TLR2 agonists induced proliferation, TLR2/1 agonist Pam3Cys and TLR2/6 agonist MALP2 were compared (Fig. 4C; Supplementary Fig. 4SE). Only Malp2 induced proliferation indicating TLR2/6 heterodimers were likely key to signaling.

The *in vitro* assay afforded the opportunity to eliminate the role of PAFr in transport of CW across the blood brain barrier and to dissect the role of the pneumococcal teichoic acid component of the cell wall in proliferation. A much stronger decrease in proliferation in PAFr TLR2 double knock out cells compared to single knock outs (Supplementary Fig.

4SA) suggested a role for both receptors in signaling proliferation. The attenuation of proliferation by EA CW or PAFr$^{-/-}$ cells in vitro also suggested at least some role for PAFr in proliferation (Supplementary Fig. 4SE).

Consistent with *in vivo* findings, CW associated with the neuronal surface and within cells *in vitro* (Fig. 4D). Neurons also produced significantly longer neurites in response to CW, a response comparable to the positive control VEGF (Fig. 4E). Stimulated NPCs showed increased expression of p-AKT and PI3Kinase (Fig. 4F). CW failed to induce the glial activation marker Iba-1 or secretion of inflammatory cytokines into the NPC supernatant fluid (Fig. 4G). Thus CW failed to induce TLR2/1 inflammatory markers or glial activation but induced mediators characteristic of the alternative TLR2/6 pathway in neuronal cells.

Interactions between CW and FoxG1 signaling

The neuronal nuclear transcription factor FoxG1 maintains progenitor cells (Dastidar et al., 2011; Regad et al., 2007) and is required for patterning of the telencephalon (Hebert and Fishell, 2008), neural cell transit through the cortex (Miyoshi and Fishell, 2012), and regulation of neural precursor proliferation (Martynoga et al., 2005). As these phenotypes were altered by CW, we tested if FoxG1 participated in the effects of CW on neuronal fate. When embryos were exposed to CW at E15, FoxG1 expression was strongly enhanced within 6 hrs of CW exposure, especially in the cortical plate (Fig. 5A). This response was sustained for up to 24 hrs and was similar in E10 embryos (data not shown). In contrast, FoxG1 expression was significantly muted in TLR2$^{-/-}$ or PAFr$^{-/-}$ embryos challenged with CW (Fig. 5A). FoxG1 staining co-localized with the expression of neuronal markers NeuN and tubulin β-III (Fig 5B, Supplementary Fig. 5SA). Adjacent brain sections demonstrated strong induction of expression of PI3kinase, a protein in the FoxG1 signaling cascade (Supplementary Fig. 5SB). Induction of FoxG1 required CW entry into the brain since challenge with EA CW failed to induce enhanced FoxG1 staining (Fig. 5C). In vitro challenge of NPCs indicated that induction of FoxG1 expression was dependent on CW dose (Fig. 5D). Taken together, these data suggest that FoxG1, an important regulatory transcription factor that has central significance in the development of the fetal cortex, is strongly enhanced in the embryonic brain after CW exposure. Furthermore, CW induced signaling via TLR2 played a role in the increased expression of FoxG1 in the fetal brain.

Behavioral consequences of fetal exposure to pneumococcal CW

In humans and postnatal mice, pneumococcal meningitis often results in neuronal loss with subsequent impaired memory and cognitive function (Grandgirard et al., 2007; Schmidt et al., 2006; Tauber et al., 2009). In contrast, our data suggest that, within the fetal cortex, CW enhances proliferation of neurons leading to an increase in overall number of neurons in the cortical plate. We sought to determine if this increased proliferation affected postnatal behavior as assessed by three assays of spatial learning and working memory (Supplementary Fig. 6S). In the spatial recognition format, the time spent examining novel arms of the maze was significantly less time for pups exposed to CW at E10 (Fig. 6A). In the delayed non-matched to position Y maze test, pups were tested for working memory sequentially over weeks postnatally (Fig. 6B). Between 6–9 weeks of age, the PBS exposed mice improved memory function as denoted by an increase in the percentage of novel

choices while the CW exposed mice made significantly fewer novel choices as they aged. These data suggest that the increased neuronal density in the cortical plate after early exposure to CW *in utero* (i.e. E10) was associated with a detrimental effect on the memory and cognitive function of postnatal mice.

To determine if the timing of CW challenge during pregnancy affected subsequent cognitive deficits, mothers were challenged with CW at E10 or E15. The pups were carried to term and tested in the Novel Object Recognition test of memory and anxiety at 3 months of age. E10 challenged pups demonstrated significantly less exploration measured as total time, time with an old object or time with a new object (Fig. 6C). E15 challenged pups showed no differences from PBS controls. Thus, although CW challenge at E10 but not E15 induced proliferation *in vivo* and was associated with subsequent behavioral abnormalities.

Discussion

The maternal-fetal environment shapes the development and long-term function of the fetal brain, including the consequences of exposure *in utero* to inflammatory or infectious stimuli. The peptidoglycan-teichoic acid complex of bacterial CW is a potent library of bioactive components that interacts with innate immune receptors to generate inflammation during infection. In the postnatal setting, CW engages PAFr to translocate across endothelial barriers from blood into brain, a process that is also operative at the placental and fetal blood brain barrier. Once in the brain in the postnatal setting, CW interacts with TLR2 engendering an intense acute phase inflammatory response recognized clinically as meningitis. Our data indicate that the TLR2-dependent response to this PAMP in the fetus is fundamentally distinct from the postnatal scenario. Inflammation is strikingly absent in the fetal brain and TLR2-dependent neuronal death is dramatically mitigated. Furthermore, the developing fetal brain responds with neuroproliferation. CW trafficked quickly from the maternal circulation to the fetal brain and then appeared to be cleared over the course of several days. Within 24hrs of CW exposure, proliferation of new neurons was prominent in the ventricular zone of the cortex. Exposure early in gestation (E10) engendered proliferation sufficient to increase neuronal density in the cortical plate at E16. This suggests that immature neurons underwent proliferation in the ventricular zone and then migrated to and accumulated in the cortical plate over time. E15 challenge with E16 histopathology showed no increase in cortical plate neuronal density suggesting either the window for the effect closes late in gestation, or the new neurons did not have time to migrate to the cortex within 24 hrs.

After injury to the postnatal brain, a repair response is limited. Modulation of the brain repair response so as to improve neurogenesis has been sought to improve the outcome of affected patients. For instance, apoptosis can be prevented by increased signaling via fas-apoptotic inhibitory molecule 2 (Reich et al., 2011) or by administration of caspase inhibitors (Braun et al., 1999). Alternatively, some induction of neurogenesis in adult hippocampal cells has been seen by enhancing signaling via TLR2, decreasing signaling by TLR4 (Rolls et al., 2007) or by blockade of IL-6 (Monje et al., 2003). In contrast, TLR2 signaling induced by synthetic ligands in the embryonic brain (E15) has been shown to decrease neuronal proliferation associated with enlarged cerebral ventricles (Okun et al.,

2010). Our data indicate that a strong neurogenerative response occurs in the early fetal brain upon challenge with bacterial PAMPs recognized by TLR2 and this response involves a previously unrecognized link between TLR2 and the neuronal transcription factor FoxG1.

FoxG1 is a transcription factor required for development and patterning of the telencephalon in the embryo (Danesin et al., 2009; Hebert and Fishell, 2008; Manuel et al., 2010; Martynoga et al., 2005) and has been referred to as a spatio-temporal hub gene in the brain. Dysregulation of FoxG1 is associated with medulloblastoma (Adesina et al., 2007), impaired neurogenesis (Shen et al., 2006) and autism spectrum disorder (Mariani et al, 2015). Recent studies have also implicated FoxG1 in promoting survival in differentiated, post-mitotic neurons (Dastidar et al., 2011). Our data show that fetal CW exposure greatly enhanced FoxG1 expression in both immature neurons of the ventricular zone and particularly in post-mitotic neurons in the cortical plate. Neuroproliferation could arise by the known ability of FoxG1 to antagonize the cytostatic signal of TGFβ-FoxO-Smad proteins (Chan et al., 2009; Seoane et al., 2004).

CW-induced neuroproliferation and enhanced FoxG1 expression were both dependent on TLR2. TLR2 is a heterodimer with TLR1 or TLR6 (Fukao and Koyasu, 2003). CW/TLR2/1 is known to induce inflammation via MyD88 activation of NFkb but this canonical pathway was not strongly activated in the fetus as evidenced by the striking lack of inflammation in the CW exposed fetal brain and the absence of in vitro neuroproliferation in response to the TLR2/1 agonist. More recently, it has been shown that TLR2/6 down regulates inflammation and induces cell proliferation by signaling via PI3 Kinase and p-AKT (Fukao and Koyasu, 2003). Exposure of NPCs or fetal brains to CW induced PI3 Kinase, p-AKT and neuroproliferation. PI3 Kinase, like FoxG1, antagonizes the cytostatic signal of TGFβ-FoxO-Smad proteins (Chan et al., 2009; Seoane et al., 2004). Thus, FoxG1 and TLR2/6 signaling could converge on TGFβ-FoxO-Smad to alleviate cytostasis. It is also possible that there is an as yet unknown direct link between TLR2 and FoxG1 given the TLR2 dependence of the CW-induced increase in FoxG1 expression in vivo. It is possible that the fetal brain escapes cell death and inflammation while inducing neuroproliferation by TLR2/6 mediated signaling in contrast to the postnatal TLR2/1 scenario.

Neuroproliferation, which occurs variably throughout life (van Praag et al., 2002), is a necessary step toward brain repair. The accumulation of neurons however, may not assure appropriate integration into functioning neuronal circuitry (Scharfman and Hen, 2007). For instance, Bax-deficient mice exhibit excess neurons leading to altered neuroanatomy and behavioral deficits (Buss and Oppenheim, 2004; Kim et al., 2009). Our data indicate a similar outcome in the setting of CW exposure in that expansion of mature neurons in the cortical plate was associated with abnormalities in learning and memory and social behavior between 6 weeks and 5 months after birth. It has been shown that the balance of pro- and anti-inflammatory signals present during fetal development can have an effect on later cognitive function (Fukao and Koyasu, 2003). While a specific mechanism for cognitive and behavioral abnormalities as a result of fetal exposure to CW is unknown, our data suggest that changes in the balance of neuroproliferation and cell death in the developing brain likely contribute to a final outcome of altered brain function in mice exposed to CW *in utero*.

The similarity of the fetal neuroproliferative response between the CW challenge model and the live infection model raises the possibility that the use of bacteriolytic antibiotics during pregnancy may have significant untoward effects on embryogenesis. On the other hand, there is a potential beneficial clinical relevance in understanding the timing and mechanism by which TLR2 drives neuroproliferation in the fetal brain to efforts to improve brain repair.

Experimental Procedures

Animals

Wild type C57BL/6 (The Jackson Laboratory), PAFr$^{-/-}$ (Radin et al., 2005), TLR2$^{-/-}$ (Yoshimura et al., 1999), FUCCI (Sakaue-Sawano et al., 2008), and Nestin promoter GFP-transgenic mice (Yamaguchi et al., 2000) were used in designated experiments. Nestin-GFP mice were backcrossed >6 times with PAFr$^{-/-}$ and TLR2$^{-/-}$ mice for use in neurogenesis experiments. All mice were maintained in the St. Jude Animal Resource Center BSL 1 and 2 housing, and all experiments were carried out in accordance with institutional guidelines and NIH protocols. Timed pregnancies were determined by ultrasound.

Placental health was monitored by pulse-wave doppler measurements were obtained using a VEVO-770 High Resolution Ultrasound System (VisualSonics, Toronto, Canada) equipped with a RMV-706 (40MHz) transducer operating at a transmit frequency of 30 MHz. Pulse-wave (PW) Doppler mode was then used to determine flow within the target umbilical cord prior to treatment and at fixed time-points after intravenous administration of pneumococcal CW. For post-processing of each data set, maternal heart rate was determined from the real-time ECG over a 10-beat period. Umbilical flow was similarly determined over 5 cycles and built-in calibrated software tools were used to determine both fetal heart rate and umbilical vein blood flow velocity.

Behavioral testing

Working memory of WT CW treated mice was tested as previously described using three assays (Bevins and Besheer, 2006; Crawley, 2007): novel object recognition, spatial recognition and delayed non-matched to position tests. For *Novel Object Recognition,* mice underwent testing at 3 months of age as previously described. Briefly, mice were acclimated to a clear field in a dimly lit room for 5 minutes on Day 1. On Day 2, mice were presented with two of the same object (red glass diamond) in the boxed field and allowed to explore for 3 minutes. On Day 3, one old object and one new object (white porcelain rectangle) were placed in the field and mice were allowed to explore for 2 minutes. Time spent at each object on Days 2 and 3 was recorded by video. Discrimination indices were determined by the equation: (New Object − Old Object)/Total Time. *For spatial recognition*, a Y-maze test was conducted in a three-arm maze made from white opaque polyvinyl plastic. The mice were exposed to the start and open arms for 8 minutes. The novel arm was gated. After one hour, each mouse was exposed to all three arms for 5 minutes. Total exploration time in each arm was noted. For *delayed non-matched to position*, water deprived mice were exposed for 10 minutes to all 3 arms of the Y maze, the open and novel arms containing chocolate milk. The following day mice were allowed access to the start arm and an open arm. Once the mouse reached the open arm, it was returned to the start and the gate for the novel arm was

lifted. A correct choice was made if the mouse initially entered the novel arm. This test was repeated randomly switching which arm was gated.

Pneumococcal Cell Wall Purification and Mouse Challenge

Highly purified CW was prepared as described previously from *Streptococcus pneumoniae* unencapsulated strain R6 (Tuomanen et al, 1985a and b) and tested endotoxin free by Limulus gel assay (Genscript). This method results in multimeric peptidoglycan with attached teichoic acid that is free of protein adducts and lipid contaminants as determined by HPLC and mass spectrometry of subcomponents (Garcia Bustos et al, 1987). The same procedure was used to purify EA CW from cultures grown in media substituting ethanolamine for choline resulting in modification of the aminoalcohol on the teichoic acid. These preparations have been studied extensively as biologically active and structurally defined TLR2 ligands (Yoshimura et al, 1999). Staphylococcal peptidoglycan was purchased (Sigma). For mouse challenge, CW was suspended in PBS, sonicated, and administered intravenously to pregnant dams as 2×10^7 bacterial equivalents. For some experiments, CW was directly labeled with 1mg/ml FITC (fluorescein isothiocyanate; Sigma) in carbonate buffer (pH 9.2) for 30min at RT in the dark and washed twice with PBS. Unless otherwise noted, dams were challenged at E10 and fetal brains were harvested at E16.

For live maternal infection and antibiotic treatment, dams at E9 were given 3×10^6 cfu *S. pneumoniae* strain TIGR4X *pln-* intratracheally; pneumolysin negative mutant was chosen to eliminate effects of the toxin on the CW phenotype. The course of systemic infection was monitored over 24 hours by Xenogen imaging and blood titers were obtained to assure consistent bacterial load (mean 5×10^5 cfu/ml). The dams were then treated with either ampicillin (100mg/kg PO every 12 hours) or clindamycin (15mg/kg PO every 12 hours) until E16 when embryos were harvested for analysis of cortical morphology.

Histology

Fetal brains and placenta were fixed in 3% paraformaldehyde (PFA) and then rehydrated in 30% sucrose. Cryosections were cut to 20μm and stained for histology by Haematoxylin and Eosin (Sigma) or Vectastain ABC kit (Vector Laboratories). Sections were treated with antibodies to FoxG1 (AbCam), TLR2 (Sigma), PAFr (Santa Cruz Biotech), phosphohistone H3 (Cell Signaling), NeuN (Millipore), Iba1 (Abcam), Tubulin III (Millipore) and fluorescent secondary antibody (Invitrogen). Methyl green (Vector Laboratories), Alexa Fluor 568 (Invitrogen) or Prolong Gold with DAPI (Molecular Probes) were used as counterstain. For TUNEL (Millipore) and Caspase-3 (Cell Signaling) positive cell counts, the area of the cortex was measured and individual positive cells were counted. Immunofluorescent sections were imaged using a Zeiss LSM 510 NLO Meta microscope equipped with HeNe, Argon/2 and Chameleon lasers. Confocal images were analyzed using Zen 2008 software. Histology sections for brightfield imaging were obtained with a Nikon E800 microscope. Image analysis, including MFI determination, was done using ImageJ software.

Stereology

Calculations of cortical area and cell number per cortex were based on standard stereology methods using the Microbrightfield StereoInvestigator with Cavalieri estimator and the optical fractionator probe, respectively (MBF Biosciences, Williston, VT). Briefly, closely matched paraffin-embedded sagittal sections (three per embryo) of the right cortex were stained with cresyl violet and the average area and cell number were calculated per mouse. Measurements were performed on five to seven animals in each experimental group.

In vitro analysis of embryonic NPCs and trophoblast cells

Embryonic NPCs were cultured from WT, PAFr$^{-/-}$ or TLR2$^{-/-}$ dams at E12, E14, or E16 using NB27 medium (Life Technologies). Briefly, brains were digested in 6 mg/mL papain (Sigma) for 30 minutes at 37°C. Tissue was washed twice before sequential trituration in culture media. Dispersed cells were spun, resuspended at 5×10^5 cells/mL, and plated on poly-D-lysine (Sigma) coated plates. For in vitro proliferation assays, cells were stained while in suspension using CellTrace CFSE Proliferation kit according to manufacturers protocol (Molecular Probes). One day after plating, cells were treated with CW at a MOI of 10. 48 hours later, cells were gently harvested by cell scraper and analyzed by FACS Canto II (Becton Dickinson). For challenge with lytic debris of living bacteria, the pneumolysin deficient mutant TIGR4 *pln*- was grown to 10^6 cfu/ml, treated with 10x MIC of ampicillin or clindamycin for 20 min and then applied to NPCs. In some cases, JEG-3 choriocarcinoma cell line ATCC HTB-36 was substituted to represent placental trophoblast cells.

Two assays were used to confirm the CSFE assay. Cell number was quantitated manually by counting in a hemocytometer. Proliferation was also measured by incorporation of BrdU (EMD Millipore). NPC's were seeded in 96 well plates and treated with CW the next day. Three days later, BrdU was added and, 24 hours later, the cells were fixed and analyzed according to the manufacturer's protocol.

To visualize CW interactions with neurons, NPCs were exposed to FITC-labeled CW for 48 h, fixed with 3% (v/v) PFA and visualized by confocal microscopy. Extracellular CW was stained with anti-FITC goat sera (Invitrogen) without permeabilization, followed by Alexa Fluor 647-conjugated chicken anti-goat sera (Invitrogen). For identification of neuronal cells, cells were stained with rabbit anti-NeuN sera (Abcam) in the presence of 0.2% (v/v) saponin, followed by Alexa Fluor 568-conjugated donkey anti-rabbit sera (Invitrogen).

To determine CW effects on outgrowth of neurites, NPCs were stimulated with CW (MOI of 10), positive control VEGF (5nM) or PBS. 24 hours post-stimulation, cultures were fixed and immunolabeled with NeuroD1 antibody and an Alexa 488 conjugated secondary antibody. Cultures were imaged with a spinning disc confocal at 40x, and length of individual neurites was measured in Slidebook. Neurons with individually resolveable neurites longer than cell body size were analyzed.

Protein expression in CW treated NPCs was analyzed by western blot. Cells were lysed 5 minutes on ice using NPer neuronal protein extraction buffer (Thermo Scientific), gently scraped and spun. Supernatant was harvested and total protein was quantitated. Undiluted

supernatants were analyzed for cytokine levels using mouse IL-6 and CXCL1/KC ELISA kits (R&D Systems) according to manufacturers protocol.

Statistics

All statistics were done using GraphPad Prism (GraphPad). Two-tailed T-tests with Welch's correction, Mann-Whitney, and 2-way Anova tests were done as noted.

Supplementary Material

Refer to Web version on PubMed Central for supplementary material.

Acknowledgments

The authors would like to thank the St. Jude Animal Resource Center and St. Jude Small Animal Imaging Center, especially Dr. Chris Calabrese and Melissa Johnson, RLAT, for help with timed matings and ultrasound data collection and analysis. We thank the St. Jude Cell and Tissue Imaging Center for microscopy assistance (supported by SJCRH and NCI P30 CA021765-35). We thank Drs. Masahiro Yamaguchi and Atushi Miyawaki from the RIKEN Institute, Japan for the FUCCI mice. We thank St Jude colleagues Donnie Eddins for his advice on the animal behavior analysis and Dr. Justin Thornton for review of the manuscript. PM was supported by NCI R25 CA23944; ET was supported by NIAID R0127913 and ALSAC.

References

Adesina AM, Nguyen Y, Mehta V, Takei H, Stangeby P, Crabtree S, Chintagumpala M, Gumerlock MK. FOXG1 dysregulation is a frequent event in medulloblastoma. J Neurooncol. 2007; 85:111–122. [PubMed: 17522785]

Aliprantis AO, Yang RB, Mark MR, Suggett S, Devaux B, Radolf JD, Klimpel GR, Godowski P, Zychlinsky A. Cell activation and apoptosis by bacterial lipoproteins through toll-like receptor-2. Science. 1999; 285:736–739. [PubMed: 10426996]

Bevins RA, Besheer J. Object recognition in rats and mice: a one-trial non-matching-to-sample learning task to study 'recognition memory'. Nature Protocols. 2006; 1:1306–1311. [PubMed: 17406415]

Braun JS, Novak R, Herzog KH, Bodner SM, Cleveland JL, Tuomanen EI. Neuroprotection by a caspase inhibitor in acute bacterial meningitis. Nat Med. 1999; 5:298–302. [PubMed: 10086385]

Braun JS, Novak R, Murray PJ, Eischen CM, Susin SA, Kroemer G, Halle A, Weber JR, Tuomanen EI, Cleveland JL. Apoptosis-inducing factor mediates microglial and neuronal apoptosis caused by pneumococcus. J Infect Dis. 2001; 184:1300–1309. [PubMed: 11679919]

Buss RR, Oppenheim RW. Role of programmed cell death in normal neuronal development and function. Anat Sci Int. 2004; 79:191–197. [PubMed: 15633457]

Canetta S, Sourander A, Surcel HM, Hinkka-Yli-Salomäki S, Leiviskä J, Kellendonk C, McKeague IW, Brown AS. Elevated maternal C-reactive protein and increased risk of schizophrenia in a national birth cohort. Am J Psychiatry 2014. 2014; 171:960–968.

Chan DW, Liu VW, To RM, Chiu PM, Lee WY, Yao KM, Cheung AN, Ngan HY. Overexpression of FOXG1 contributes to TGF-beta resistance through inhibition of p21WAF1/CIP1 expression in ovarian cancer. Br J Cancer. 2009; 101:1433–1443. [PubMed: 19755996]

Clarke TB, Davis KM, Lysenko ES, Zhou AY, Yu Y, Weiser JN. Recognition of peptidoglycan from the microbiota by Nod1 enhances systemic innate immunity. Nat Med. 2010; 16:228–231. [PubMed: 20081863]

Collins SM, Surette M, Bercik P. The interplay between the intestinal microbiota and the brain. Nat Rev Microb. 2012; 10:735–742.

Couzin-Frankel J. Mysteries of development. How does fetal environment influence later health? Science. 2013; 340:1160–1161. [PubMed: 23744922]

Crawley JN. Mouse Behavioral Assays Relevant to the Symptoms of Autism. Brain Pathology. 2007; 17:448–459. [PubMed: 17919130]

Cryan JF, Dinan TG. Mind-altering microorganisms: the impact of the gut microbiota on brain and behaviour. Nat Rev Neurosci. 2012; 13:701–712. [PubMed: 22968153]

Cundell DR, Gerard NP, Gerard C, Idanpaan-Heikkila I, Tuomanen EI. Streptococcus pneumoniae anchor to activated human cells by the receptor for platelet-activating factor. Nature. 1995; 377:435–438. [PubMed: 7566121]

Danesin C, Peres JN, Johansson M, Snowden V, Cording A, Papalopulu N, Houart C. Integration of telencephalic Wnt and hedgehog signaling center activities by Foxg1. Dev Cell. 2009; 16:576–587. [PubMed: 19386266]

Dastidar SG, Landrieu PMZ, D/Mello SR. FoxG1 Promotes the Survival of Postmitotic Neurons. J Neurosci. 2011; 31:402–413. [PubMed: 21228151]

Fillon S, Soulis K, Rajasekaran S, Benedict-Hamilton H, Radin JN, Orihuela CJ, El Kasmi KC, Murti G, Kaushal D, Gaber MW, et al. Platelet-activating factor receptor and innate immunity: uptake of gram-positive bacterial cell wall into host cells and cell-specific pathophysiology. J Immunol. 2006; 177:6182–6191. [PubMed: 17056547]

Fukao T, Koyasu S. PI3K and negative regulation of TLR signaling. Trends Immunol. 2003; 24:358–363. [PubMed: 12860525]

Garcia-Bustos JF, Chait BT, Tomasz A. Structure of the peptide network of pneumococcal peptidoglycan. J Biol Chem. 1987; 262:15400–15405. [PubMed: 2890629]

Gerber J, Bottcher T, Bering J, Bunkowski S, Bruck W, Kuhnt U, Nau R. Increased neurogenesis after experimental Streptococcus pneumoniae meningitis. J Neurosci Res. 2003; 73:441–446. [PubMed: 12898528]

Grandgirard D, Steiner O, Tauber MG, Leib SL. An infant mouse model of brain damage in pneumococcal meningitis. Acta neuropath. 2007; 114:609–617. [PubMed: 17938941]

Hebert JM, Fishell G. The genetics of early telencephalon patterning: some assembly required. Nat Rev Neurosci. 2008; 9:678–685. [PubMed: 19143049]

Hoffmann O, Mahrhofer C, Rueter N, Freyer D, Bert B, Fink H, Weber JR. Pneumococcal cell wall-induced meningitis impairs adult hippocampal neurogenesis. Infect Immun. 2007; 75:4289–4297. [PubMed: 17591796]

Hsiao EY, McBride SW, Hsien S, Sharon G, Hyde ER, McCue T, Codelli JA, Chow J, Reisman SE, Petrosino JF, et al. Microbiota modulate behavioral and physiological abnormalities associated with neurodevelopmental disorders. Cell. 2013; 155:1451–1463. [PubMed: 24315484]

Kim WR, Park OH, Choi S, Choi SY, Park SK, Lee KJ, Rhyu IJ, Kim H, Lee YK, Kim HT, et al. The maintenance of specific aspects of neuronal function and behavior is dependent on programmed cell death of adult-generated neurons in the dentate gyrus. Eur J Neurosci. 2009; 29:1408–1421. [PubMed: 19519627]

Lowe GC, Luheshi GN, Williams S. Maternal infection and fever during late gestation are associated with altered synaptic transmission in the hippocampus of juvenile offspring rats. Am J Physiol Reful Inter Comp Physiol. 2008; 195:R1563–R1571.

Manuel M, Martynoga B, Yu T, West JD, Mason JO, Price DJ. The transcription factor Foxg1 regulates the competence of telencephalic cells to adopt subpallial fates in mice. Development. 2010; 137:487–497. [PubMed: 20081193]

Mariani J, Coppola G, Shang P, Abyzov A, Provini L, et al. FOXG1-dependent dysregulation of GABA/glutamate neuron differentiation in autism spectrum disorders. Cell. 2015; 162:375–390. [PubMed: 26186191]

Martynoga B, Morrison H, Price DJ, Mason JO. Foxg1 is required for specification of ventral telencephalon and region-specific regulation of dorsal telencephalic precursor proliferation and apoptosis. Dev Biol. 2005; 283:113–127. [PubMed: 15893304]

Mitchell L, Smith SH, Braun JS, Herzog KH, Weber JR, Tuomanen EI. Dual phases of apoptosis in pneumococcal meningitis. J Infect Dis. 2004; 190:2039–2046. [PubMed: 15529270]

Miyoshi G, Fishell G. Dynamic FoxG1 expression coordinates the integration of multipolar pyramidal neuron precursors into the cortical plate. Neuron. 2012; 74:1045–1058. [PubMed: 22726835]

Monje M, Toda H, Palmer T. Inflammatory blockade restores adult hippocampal neurogenesis. Science. 2003; 302:1760–1765. [PubMed: 14615545]

Nau R, Bruck W. Neuronal injury in bacterial meningitis: mechanisms and implications for therapy. Trends Neurosci. 2002; 25:38–45. [PubMed: 11801337]

Okun E, Griffioen KJ, Gen-Son T, Lee JH, Roberts NJ, Mughal MR, Hutchison E, Cheng A, Arumugam TV, Lathia JD, vanPraag H, Mattson MP. TLR2 activation inhibits embryonic neural progenitor cell proliferation. J Neurochem. 2010; 114:462–474. [PubMed: 20456021]

Orihuela CJ, Fillon S, Smith-Sielicki SH, El Kasmi KC, Gao G, Soulis K, Patil A, Murray PJ, Tuomanen EI. Cell wall-mediated neuronal damage in early sepsis. Infect Immun. 2006; 74:3783–3789. [PubMed: 16790750]

Radin JN, Orihuela CJ, Murti G, Guglielmo C, Murray PJ, Tuomanen EI. beta-Arrestin 1 participates in platelet-activating factor receptor-mediated endocytosis of *Streptococcus pneumoniae*. Infect Immun. 2005; 73:7827–7835. [PubMed: 16299272]

Regad T, Roth M, Bredenkamp N, Illing N, Papalopulu N. The neural progenitor-specifying activity of FoxG1 is antagonistically regulated by CKI and FGF. Nat Cell Biol. 2007; 9:531–540. [PubMed: 17435750]

Reich A, Spering C, Gertz K, Harms C, Gerhardt E, Kronenberg G, Nave KA, Schwab M, Tauber SC, Drinkut A, et al. Fas/CD95 regulatory protein Faim2 is neuroprotective after transient brain ischemia. J Neurosci. 2011; 31:225–233. [PubMed: 21209208]

Rolls A, Shechter R, London A, Ziv Y, Ronen A, Levy R, Schwartz M. Toll-like receptors modulate adult hippocampal neurogenesis. Nat Cell Biol. 2007; 9:1081–1088. [PubMed: 17704767]

Roth KA, D'Sa C. Apoptosis and brain development. Ment Retard Dev Disabil Res Rev. 2001; 7:261–266. [PubMed: 11754520]

Sakaue-Sawano A, Kurokawa H, Morimura T, Hanyu A, Hama H, Osawa H, Kashiwagi S, Fukami K, Miyata T, Miyoshi H, et al. Visualizing spatiotemporal dynamics of multicellular cell-cycle progression. Cell. 2008; 132:487–498. [PubMed: 18267078]

Scharfman HE, Hen R. Neuroscience. Is more neurogenesis always better? Science. 2007; 315:336–338. [PubMed: 17234934]

Schmidt H, Heimann B, Djukic M, Mazurek C, Fels C, Wallesch CW, Nau R. Neuropsychological sequelae of bacterial and viral meningitis. Brain. 2006; 129:333–345. [PubMed: 16364957]

Seoane J, Le HV, Shen L, Anderson SA, Massague J. Integration of Smad and forkhead pathways in the control of neuroepithelial and glioblastoma cell proliferation. Cell. 2004; 117:211–223. [PubMed: 15084259]

Shen L, Nam HS, Song P, Moore H, Anderson SA. FoxG1 haploinsufficiency results in impaired neurogenesis in the postnatal hippocampus and contextual memory deficits. Hippocampus. 2006; 16:875–890. [PubMed: 16941454]

Sorenson HJ, Mortensen EL, Reinisch JM, Mednick SA. Association between prenatal exposure to bacterial infection and risk of schizophrenia. Schizophr Bull. 2008; 35:631–637. [PubMed: 18832344]

Tauber SC, Bunkowski S, Ebert S, Schulz D, Kellert B, Nau R, Gerber J. Enriched environment fails to increase meningitis-induced neurogenesis and spatial memory in a mouse model of pneumococcal meningitis. J Neurosci Res. 2009; 87:1877–1883. [PubMed: 19170185]

Tuomanen E, Liu H, Hengstler B, Zak O, Tomasz A. The induction of meningeal inflammation by components of the pneumococcal cell wall. J Infec Dis. 1985; 151:859–868. [PubMed: 3989321]

Tuomanen EI, Tomasz A, Hengstler B, Zak O. The relative role of bacterial cell wall and capsule in the induction of inflammation in pneumococcal meningitis. J Infect Dis. 1985; 151:535–540. [PubMed: 3973407]

Tracey KJ. Reflex control of immunity. Nat Rev Immunol. 2009; 9:418–428. [PubMed: 19461672]

Yamaguchi M, Saito H, Suzuki M, Mori K. Visualization of neurogenesis in the central nervous system using nestin promoter-GFP transgenic mice. Neuroreport. 2000; 11:1991–1996. [PubMed: 10884058]

van Praag H, Schinder AF, Christie BR, Toni N, Palmer TD, Gage FH. Functional neurogenesis in the adult hippocampus. Nature. 2002; 15:1030–1034.

Yamaguchi M, Saito H, Suzuki M, Mori K. Visualization of neurogenesis in the central nervous system using nestin promoter-GFP transgenic mice. NeuroReport. 2000; 11:1991–1996. [PubMed: 10884058]

Yoshimura A, Lien E, Ingalls RR, Tuomanen E, Dziarski R, Golenbock D. Cutting edge: recognition of Gram-positive bacterial cell wall components by the innate immune system occurs via Toll-like receptor 2. J Immunol. 1999; 163:1–5. [PubMed: 10384090]

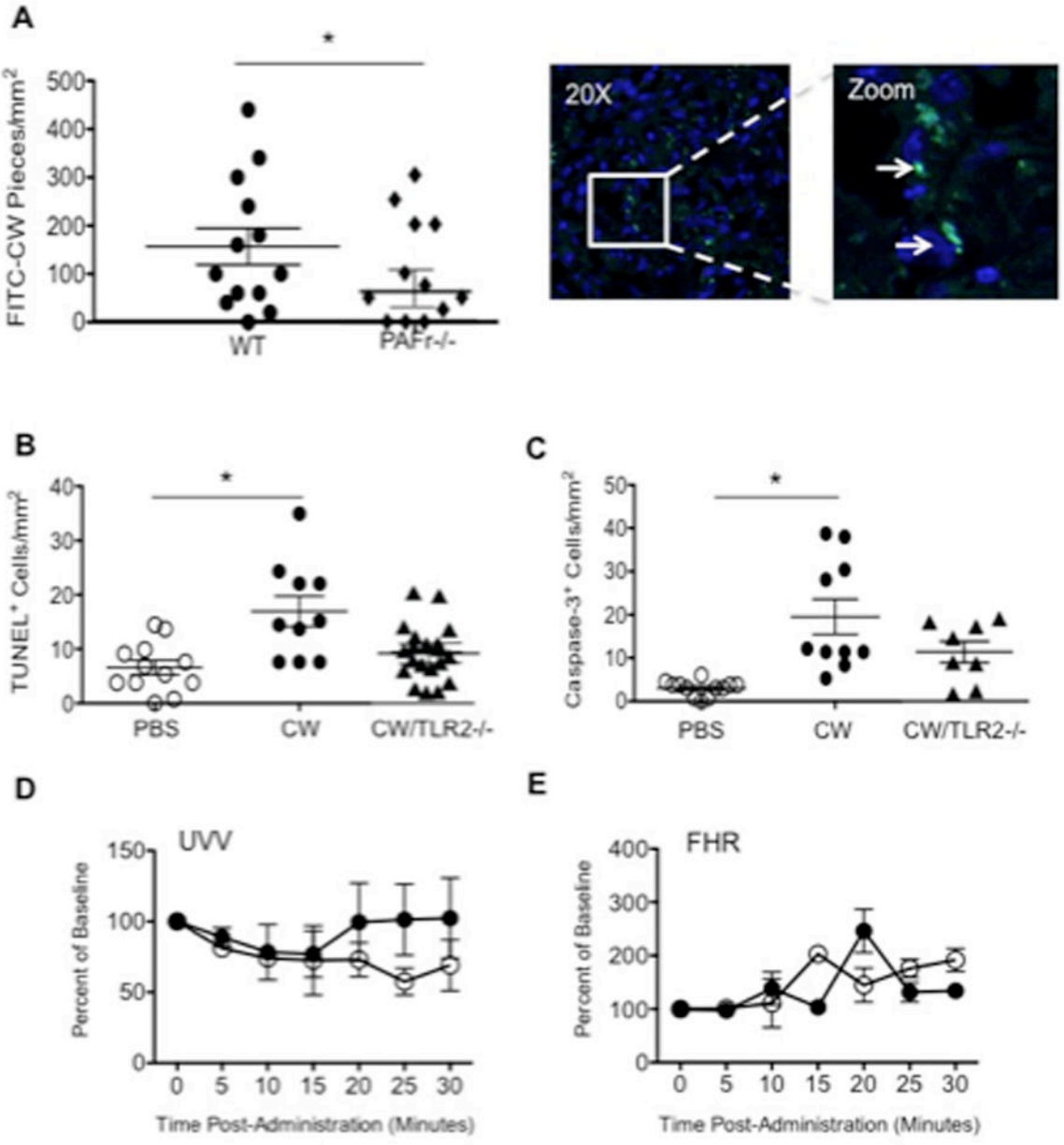

Figure 1. Interaction of CW with the placenta

FITC-labeled CW was administered IV to E15 pregnant dams and the placenta was examined 24 hours later. (A) FITC-CW pieces were visualized and enumerated in placental tissue of wild type (WT) and PAFr $^{-/-}$ dams ($p<0.005$) (green: CW; blue: nucleus). Each symbol is representative of one section, and at least 2 sections were imaged per embryo. Embryos (n= at least 8) were analyzed from at least 2 separate injections. (B, C) TUNEL^{+} ($p=0.006$) or caspase-3^{+} ($p=0.003$) cells were counted in placental tissue of WT or TLR2$^{-/-}$ dams exposed IV to CW or PBS. Each symbol is representative of one section, and at least 2 sections were imaged per embryo. Embryos ($n\geq5$) were analyzed from at least 2 separate injections. TLR2−/− values were not statistically different from PBS ($p=0.31$) (D, E) E15 pregnant dams were injected with either PBS (open circles) or CW (filled circles). Embryos

were monitored for 30 minutes immediately following injection via pulse-wave Doppler ultrasound to determine umbilical vein velocity (UVV) and fetal heart rate (FHR). For each treatment, one embryo was monitored per injection. Graphs are mean ±SEM of 3 embryos for each treatment. UVV p=0.12; FHR p>0.5. See also Figure 1S.

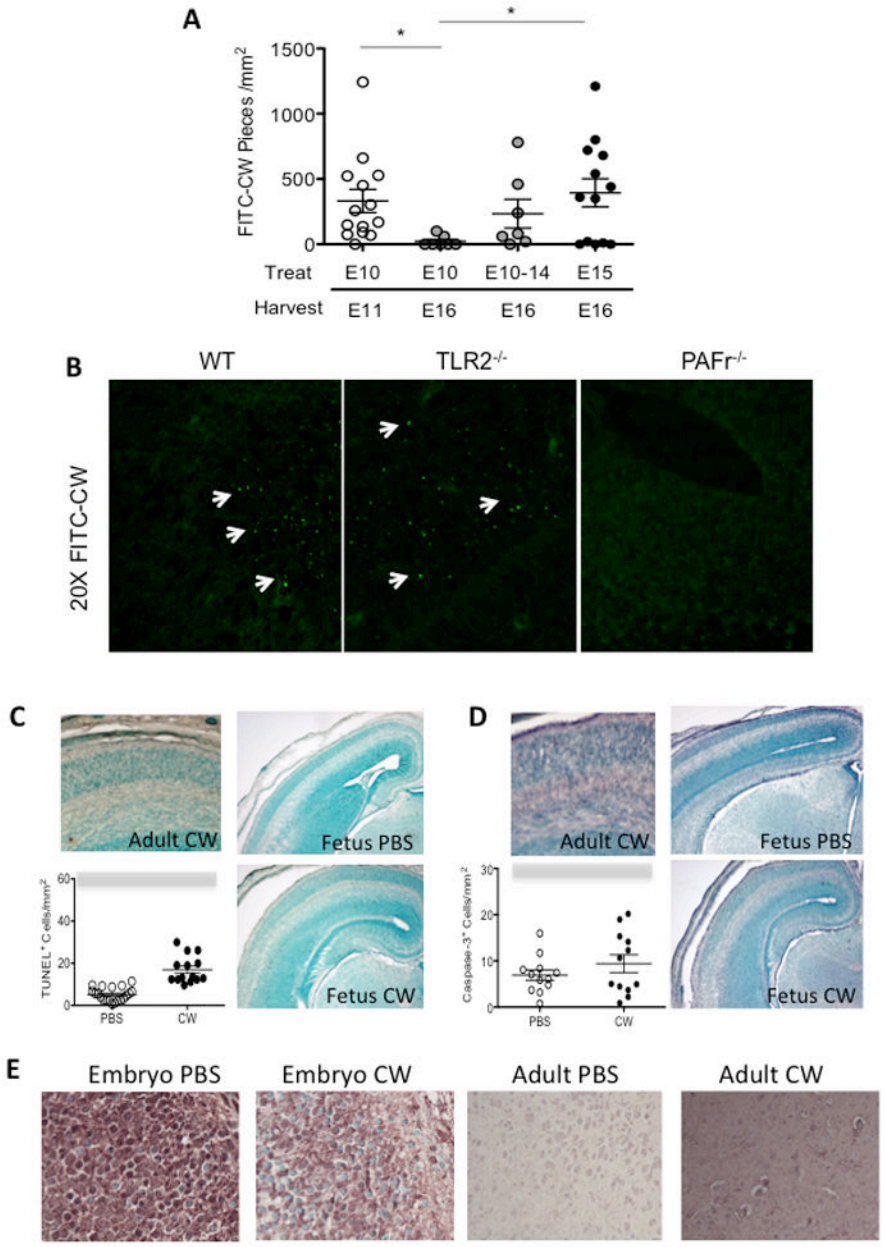

Figure 2. Interaction of CW with the fetal cortex

For all panels: Each symbol is representative of one section, and 2 or more sections were imaged per embryo or 6 wk old adult mouse. Embryos were analyzed from at least 2 separate injections for both PBS and CW treatments. (A) FITC-labeled CW was administered IV to wild-type (WT) pregnant dams at E10 or E15 in single doses, or in multiple daily doses from E10 through E14. FITC-CW pieces were enumerated in the cortex at E11 or E16 (as noted). (B) Images representative of panel A depicting FITC CW (green dots; arrows) in the cortex of WT mice 24 hrs after CW injection at E15 (20X magnification; representative of 3 slices/embryo; 3 embryos/mother; > 10 mothers). TLR2$^{-/-}$ or PAFr $^{-/-}$ mice are shown for comparison. (C, D) PBS or CW was injected IV to WT E10 pregnant dams and fetal brains were harvested at E16; as a comparison, CW was injected into 6 week

old adult mice (n=3). Graph: $TUNEL^+$ (C, $p<0.01$) or caspase-3^+ (D, $p > 0.5$) positive cells/mm^2 in the fetal cortex were enumerated at E16. Each symbol is one embryo from at least 3 different mothers; value is mean of at least 3 sections/embryo; As a comparator, the grey bars indicate mean±SD of $TUNEL^+$ (58±6) or caspase 3^+ (32±7) cells/mm^2 in adult brain. Representative 10X images. (E) Cortical sections from brain from 6 wk old mice (adult) or embryo 24hrs-post E15 PBS or CW exposure. Sections stained with anti-Iba-1 antibody, a microglial activation marker (brown), with Methyl Green (blue) as the counterstain (40X magnification). See also Figure 2S.

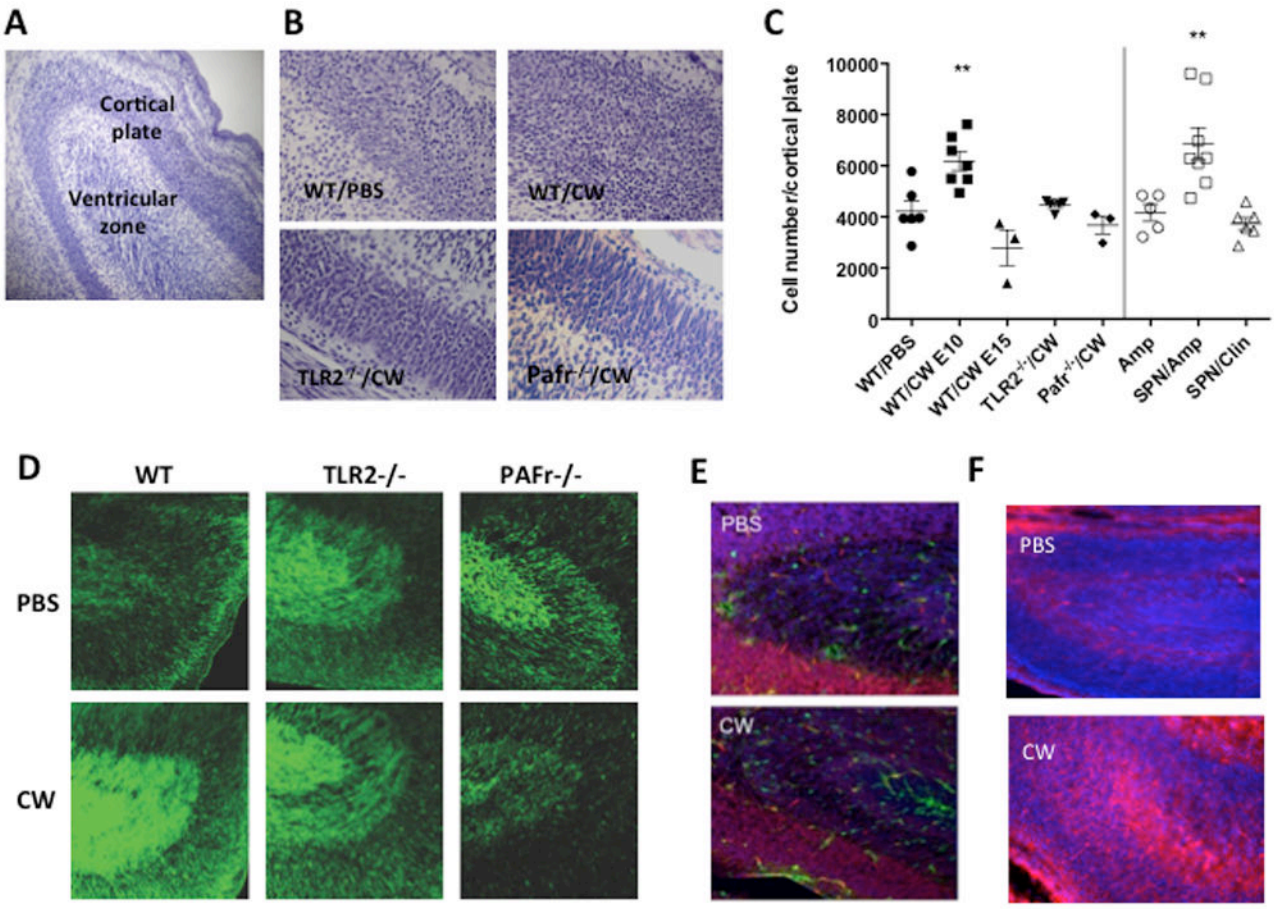

Figure 3. CW induces cortical neuronal proliferation

(A) Section of untreated control E16 fetal brain stained with cresyl violet indicating ventricular zone and cortical plate (10X magnification). (B, C left panel) Images (40X) and quantitation of cells in the cortical plate in E16 WT, TLR2$^{-/-}$, or PAFr$^{-/-}$ pups post E10 CW or PBS challenge. Challenge of WT at E15 and harvest at E16 was also quantitated. Each symbol represents the average of 3 sections counted per embryo, for 6–7 embryos/group from 3 independent experiments ($p \leq 0.004$). (C right) Quantitation of cells in the fetal cortical plate at E16 after infection of dams at E9 with *S. pneumoniae* (T4X) and treatment at E10-16 with daily ampicillin (SPN/Amp) or clindamycin (SPN/Clin). SPN/Amp vs uninfected Amp: $p = 0.009$; SPN/Clin vs SPN/Amp: $p=0.01$; (n= 3–4/group repeated twice; each symbol is one embryo). (D) Nestin-GFP WT and Nestin-GFP-TLR2$^{-/-}$ or Nestin-GFp-PAFr$^{-/-}$ transgenic pregnant dams were given either PBS or CW at E10 and GFP signal (green) was visualized at E16. (20X; representative of 3 replicates) (E) E10 pregnant FUCCI dams were given either PBS or CW and embryos were visualized at E16. Red: Cdt1^{+} cells in G1 phase of the cell cycle; Green: dividing Geminin^{+} cells in S through M phase of the cell cycle. (20X; representative of 3 replicates) (F) Cryosections of embryos given PBS or CW at E10 and harvested at E16 were examined for proliferating cells by immunofluorescence microscopy. Sections were stained with anti-phosphohistone H3 and Alexa Fluor 568 secondary antibody (pink) with Prolong Gold with DAPI (blue) as the counterstain. (20X

magnification) (representative of n=3/group; 4080±659 cells/field; 3 sections per embryo). Quantitation presented in supplementary Figure 3S.

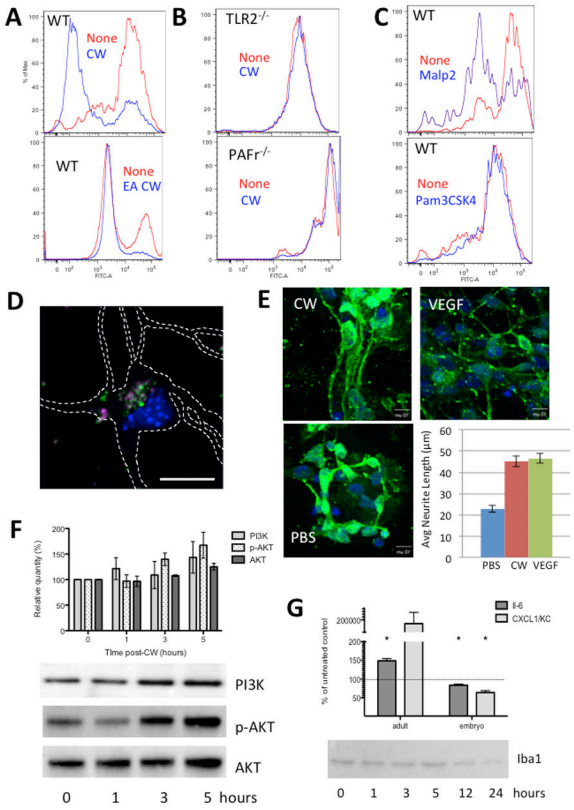

Figure 4. Neuroproliferation of neuronal precursor cells (NPCs) by CW in vitro

(A–C) Embryonic brains were harvested at E16 and NPCs were isolated, loaded with CFSE, and plated. Cells were exposed to stimuli and enumerated by FACS on Day 3. Dimming of the CFSE label indicates dilution as cells divide and shifts the peak to the left. (A) CW or EA CW vs PBS in WT or (B) TLR2$^{-/-}$ and PAFr$^{-/-}$ NPCs. Quantitation of these results is presented in Figure 4SA. (C) WT NPCs challenged with PBS, TLR1/2 agonist Pam3Cys or TLR2/6 agonist Malp2. (D) Confocal image (bar = 10 µm) showing interaction of NPC (outlined in white traced from staining with rabbit anti-NeuN) with FITC-labeled CW at 48 hrs. Extracellular (magenta) and intracellular (green) CW was differentiated as per methods. Nucleus (DAPI blue). (E) E16 NPCs were treated with PBS, CW or VEGF (positive control) for 24 hours. Confocal fluorescence microscopy was used to measure the length of neurites (NeuroD1 antibody: green; DAPI:blue). Values are mean ± SD from 3 experiments: PBS control (n=50), cell wall (n=43), and VEGF (n=46). Representative 40X images of neurons are shown. (F) Expression of PI3Kinase and p-AKT as measured by Western blot of whole cell lysate of NPCs exposed to CW varied by time (representative of 3 experiments). AKT served as loading control. Graph indicates intensity of the bands as measured by densitometry. 100% = baseline at 0 hours post PBS. (G) Lack of activation of fetal microglia in NPC preparation exposed to CW as measured by Western blot of whole cell lysate 24 hours post-CW treatment using antibody to the activation marker Iba-1 and by absence of IL-6 or CXCL1 cytokines in the supernatant as measured by ELISA. Adult NPC served as positive controls. Untreated control values set @ 100% (dashed line): IL-6 adult = 3.4 pg/mL, embryo = 15.2 pg/mL; CXCL1 adult = 0; embryo = 5.9 pg/mL. Representative of 2 experiments. See also Figure 4S.

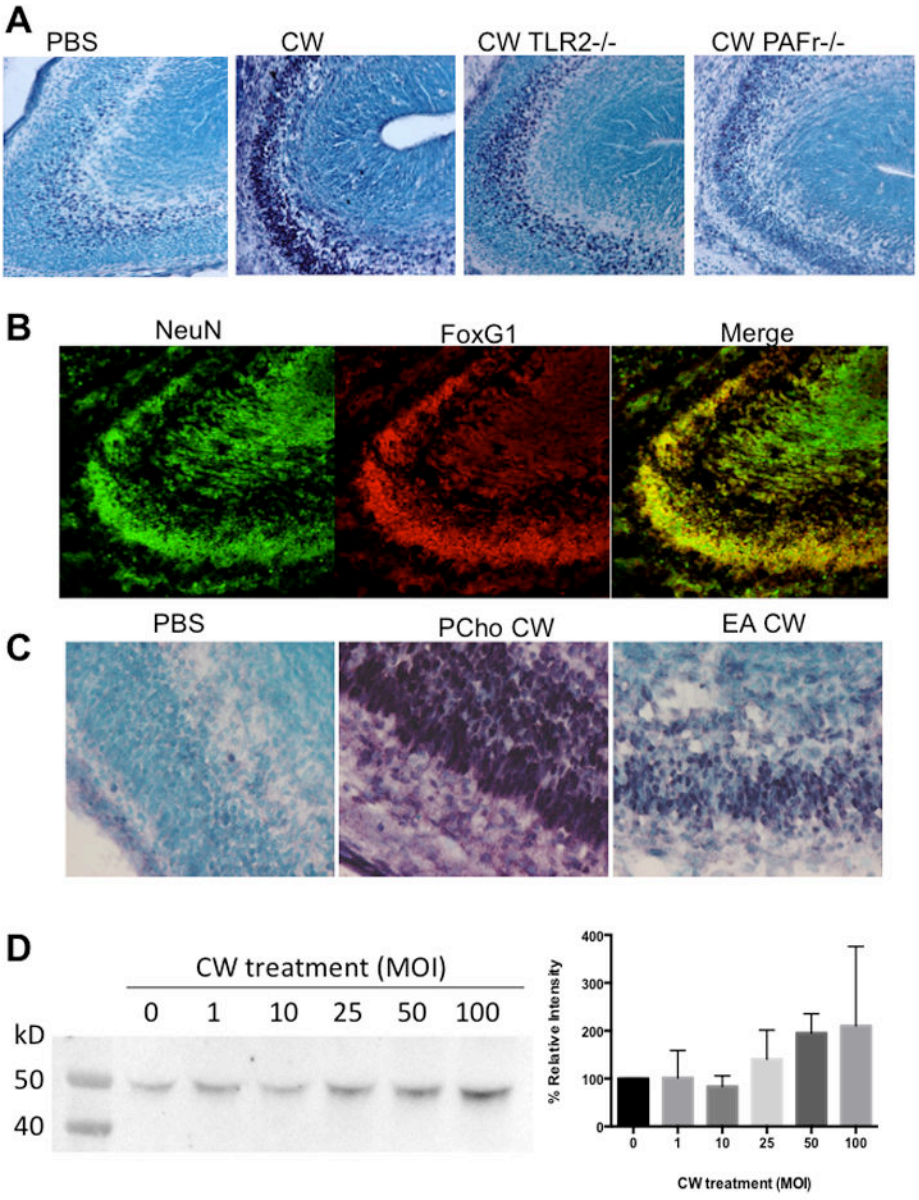

Figure 5. CW induces FoxG1 expression in the cortex

(A) E15 pregnant WT, PAFr$^{-/-}$ and TLR2$^{-/-}$ dams were given either PBS or CW intravenously. Embryos were harvested 24hrs later and the cortex was stained with antibody to FoxG1 (purple); counterstain Methyl Green (blue; 40X magnification). (B) In WT embryos, co-localization (yellow) of FoxG1 (red) with neuronal marker NeuN (green; 20X magnification) was assessed by confocal imaging. Images are representative of at least 2 independent experiments. (C) E15 pregnant WT dams were given IV wild type CW with choline in the teichoic acid (PCho CW) or CW with ethanolamine substituted for choline (EA CW). Fetal brains were stained as in A. 100X magnification; FoxG1 = purple. D) Induction of FoxG1 expression in NPCs by different doses of CW (MOI = multiplicity of infection) as measured at 8 hours by Western blot. Graph: quantification of bands by densitometry. Mean ± SD of 3 experiments. See also Figure 5S.

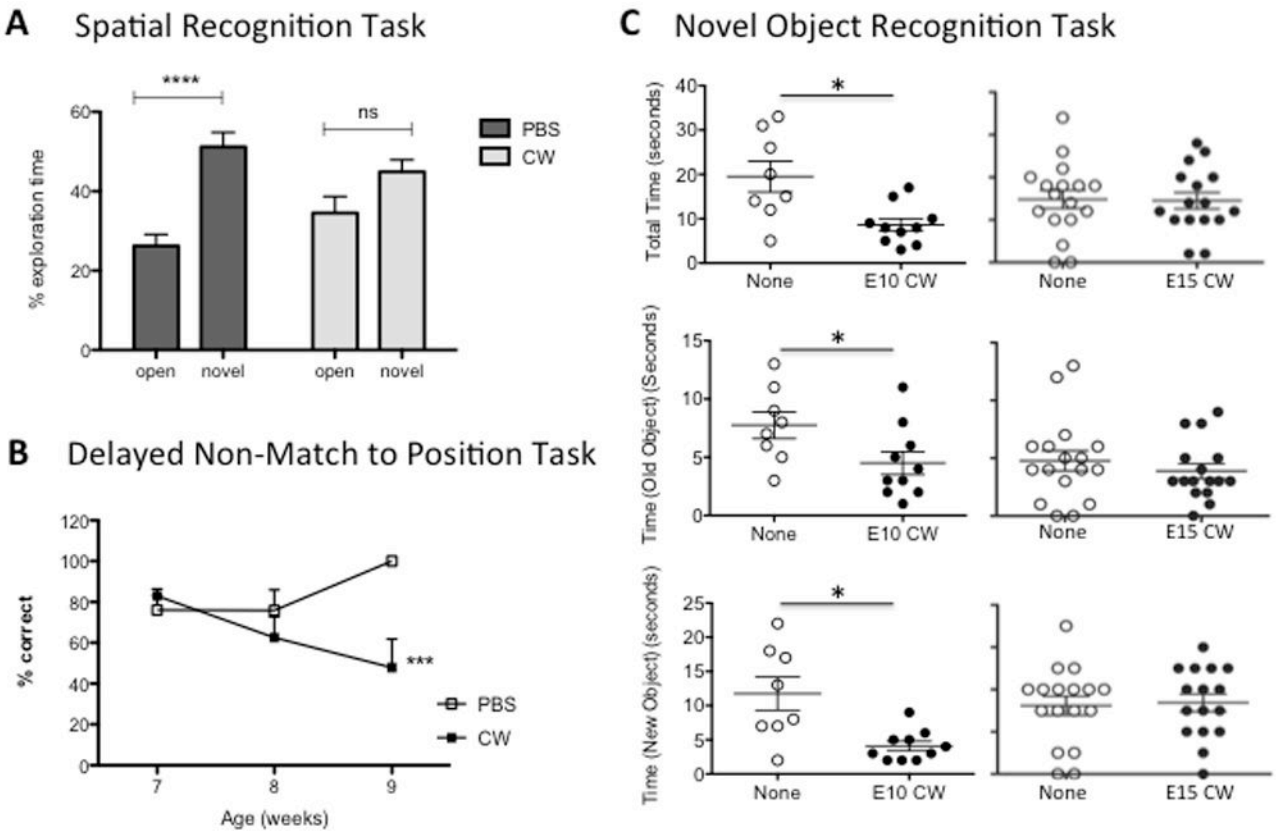

Figure 6. Early embryonic exposure to CW affects postnatal behavior

Pregnant dams were injected IV with either PBS or CW as indicated. Embryos were brought to term and between 6 weeks to 5 months of age were tested for spatial learning and working memory in three assays (see methods and Supplementary Fig 6S). (A) Spatial Recognition Task: Mothers were challenged at E10 and pups were tested at 5 months of age. Exploration of a new arm of a Y maze was measured as a % of total exploration time (5 minutes). PBS (n=10) and CW (n=16) from 2 experiments. **** $p<0.0001$. ns = no significant difference. (B) Delayed Non-match to Position Test: As in (A), the number of entries into a newly opened arm was expressed as a % of the total number of entries in 5 min. PBS (n=9); CW (n=8) from 2 experiments. *** $p= 0.006$. (C) Novel Object Recognition: E10 or E15 pregnant dams were injected IV with either PBS (n=8) or CW (n=10). At 3 mo of age pups were tested for the time exploring a new object. * $p\leq0.016$. No significant difference for E15 mice ± CW. Data combined from two experiments. See also Figure 6S.